ISSN 1560-0904, Polymer Science, Series B, 2020, Vol. 62, No. 6, pp. 602–611. © Pleiades Publishing, Ltd., 2020.

CATALYSIS

Topological and Electronic Properties of Chlorine-Substituents on the α-Diimine Ni-based Catalysts

Mostafa Khoshsefat[a], Mohsen Mogheiseh[b], Gholam Hossein Zohuri[b,*], and Saeid Ahmadjo[c]

[a] *Key Laboratory of Engineering Plastics, Beijing National Laboratory for Molecular Sciences, Institute of Chemistry, Chinese Academy of Sciences, Beijing, 100080 China*

[b] *Department of Chemistry, Faculty of Science, Ferdowsi University of Mashhad, Mashhad, 91775-1436 Iran*

[c] *Department of Catalyst, Iran Polymer and Petrochemical Institute (IPPI), Tehran, 14965/115 Iran*

**e-mail: zohuri@um.ac.ir*

Received May 5, 2020; revised July 31, 2020; accepted August 14, 2020

Abstract—The effect of substituent nature and position on a series of late transition metal catalysts based on nickel (**A**–**D**) was investigated practically and theoretically. Catalyst **A** bearing isopropyl groups on the *ortho* position showed the highest activity while for the *ortho* and *para* chlorine substituted catalysts **B**–**D** insignificant activities were observed. These experimental results were confirmed by theoretical study on the (pre)catalysts. Based on that, thermodynamics, atomic/molecular effective parameters such as bond distances, bond angles, band gap or chemical hardness, charge of Mulliken on Ni center, electronic chemical potential, global electrophilicity index and also activation energy of the pre-catalyst through the alkylation were calculated. To pursue the steric and electronic effects of substituent on the axial and equatorial sites of active center, electronic density, electron location function, localized orbital locator graphs as topological properties were studied. As a result, complex **A** with lower activation energy for alkylation, higher stability, greater Mulliken charge on Ni center and high electronic density around the active center was found as a highly active catalyst. In addition, polymerization conditions such as polymerization temperature and ethylene pressure showed significant effect on the catalysts productivity and branching density of the produced polyethylene.

DOI: 10.1134/S1560090420330039

INTRODUCTION

During two last decades after discovery of late transition metals as olefin polymerization catalysts, tremendous progress has been achieved in this field [1–3]. Theoretical and practical studies on the most class of polymerization catalysts have been carried out [4–6]. However, among these investigations, the relation between the structure and properties of the complexes is still under consideration. Theoretical studies along with the practical experiments are needed to predict the behavior of complexes or confirm the results and possible interactions [7–9].

Besides, the behavior of late transition metal complexes in (co)polymerization attracts interest due to their unique reactivity patterns and unusual catalytic properties [8]. Moreover, the effect of their structure such as metal center, multinuclearity, backbone and substituents on the polymer microstructure and properties are discussed in the literature [10–13]. For instance, Terao et al. claimed that there is a relation between the behavior of complexes and *ortho*-substituents through the distance between the atoms around the metal center [14]. Chen et al. synthesized highly active neutral single-component [N,O] chelating Ni(II) catalysts which were used in polymerization of ethylene. They mentioned that shielding of axial sites above and under the square coordination plane of Ni center greatly retards chain transfer reactions. This fact was the reason for further investigations of the possible ways of the synthesis of high molecular weight polyethylene [15]. Dai and coworkers studied the [N,N] ligand steric effect which leads to systematic tuning of the catalytic performance and polymer properties [16]. The polymerization activity enhanced gradually as the size and steric effect of ligand and substituents increased [16]. Hu et al. also disclosed that increasing of steric hindrance in the backbone of amine–imine nickel complexes results in a reduction of polymerization activity and polyethylene molecular weight [17]. Zhang and coworkers presented tridentate [O,N,O] ligand frameworks which were different in terms of *ortho*-substituents. They declared that both electron-donating and bulky *ortho*-substituents on the *N*-aryl ring significantly exert positive effects on the catalytic activities [18]. The electronic impact along with the steric effect of substituent may direct the aryl rings to inhibit the insertion of monomer into active center [19]. On the other side, the effect of electron

withdrawing groups on the catalyst behavior has been investigated. Based on this, electronegative groups such as Cl, Br, CF_3, and NO_2 on *meta* and *para* positions cause an increasing in catalyst activity and molecular weight of produced polymer [20–25]. Presence of electron donating groups on *para* position also leads to higher stability and longer lifetime of active center and producing higher molecular weight of polymer. This observation probably is due to stabilization of transition state including electrophile unsaturated alkyl species. However, electronegative groups deplete in catalyst lifetime and decrease polymer molecular weight through increasing of instability of active center and higher rate of chain transfer reactions [25]. There are also some further reports on halogenated structure of α-diimine ligands which explained the effect and mechanism of fluorine substituents on deactivation reaction [26, 27]. However less information is known for chlorine substituents which have greater size and less electronegativity. In addition to catalyst structure, reaction conditions such as cocatalyst/catalyst molar ratio, monomer concentration, polymerization time and temperature are critical factors showing high impacts on the catalyst behavior, polymerization kinetic and polymer characteristics [14, 28].

Altogether, the steric and electronic effects of aryl substituents are two key factors which can modify the metal center environment through accelerating or suppressing the polymerization reactions. Herein, we investigated the theoretical parameters such as chemical hardness η, electronic chemical potential μ, global electrophilicity index ω, electron density around the metal center, along with electronic and thermal energies to reveal and to confirm the fact of impact of structural parameters on the catalyst behavior and polymer properties. Moreover, the effect of polymerization conditions on the catalyst performance was studied.

EXPERIMENTAL

Materials

All manipulations of air and/or water sensitive compounds were conducted under argon/nitrogen atmosphere using the standard Schlenk techniques. All the solvents were purified prior to use. Toluene (purity 99.9%, Iran, Petrochemical Co.) was purified over sodium wire/benzophenone. Dichloromethane (purity 96%, Sigma Aldrich Chemicals, Germany) was purified over calcium hydride powder, and distilled prior to use as a complex synthesis solvent. Polymerization grade ethylene gas (purity 99.9%, Iran, Petrochemical Co.) was purified by passing through activated silica gel, KOH, and 4Å/13X molecular sieves column. 2,6-Diisopropylaniline, 2-chloroaniline, 2,6-dichloroaniline, 4-chloroaniline, acenaphthoquinone, nickel (II) bromide ethylene glycol dimethyl ether complex [(DME) $NiBr_2$] (purity 97%) and diethyl ether (purity 99.5%) were supplied by Merck Chemical (Darmstadt, Germany) and used in synthesis of ligands and catalysts. Decaline (decahydronaphthalene, purity 97%) was purchased from Sigma Aldrich Chemicals (Steinheim, Germany). Triisobutylaluminium (TIBA, purity 93%) was supplied by Sigma Aldrich Chemicals (Steinheim, Germany) which was used in synthesis of modified methylaluminoxane (MMAO) according to the literature [29].

Polymerization Procedure

Low pressure polymerization was carried out in a round bottom flask which was equipped with Schlenk system, vacuum line, ethylene inlet and magnetic stirrer. The high pressure (more than 2 bar) was carried out using a 1-L Buchi bmd 300 type reactor.

Characterization

^{1}H NMR and FTIR spectra were obtained using Bruker AC-80 and Bruker IF-505 spectrometers, respectively. Elemental analysis was performed on a Thermo Finnigan Flash 1112EA microanalyzer. The viscosity average molecular weight M_v of some polymer samples was determined according to the literature [30, 31]. Intrinsic viscosity [η] was measured in decaline at 133 ± 1°C using an Ubbelohde viscometer. M_v values were calculated through Mark-Houwink equation using $\alpha = 0.7$ and $K = 6.2 \times 10^{-4}$ [8]. Differential scanning calorimetry (DSC) was performed on a Q100 Perkin Elmer instrument with a heating rate of 10 grad/min. GPC curve was resulted using Agilent PL-GPC220 instruments.

Synthesis of Ligands and Catalysts

Ligands **a–d** and corresponding complexes **A–D** were synthesized according to previously reported procedure [6] (molecular structure of complexes are depicted in Fig. 1).

The characterization details of ligand **a** have been reported in our recent work [30]. Yield (yellow solid): 96%. ^{1}H NMR ($CDCl_3$, 300 MHz), δ_H, ppm: 1.0 (12H, d), 1.3 (12H, d), 3.1 (4H, s), 6.8 (2H, d) 7.4 (6H, m), 7.7 (2H, t), 8.3 (2H, d). MS (EI, *m/z*): 500 [M^+, 100%]. FTIR (KBr, cm^{-1}): 1271 (–C–N–), 1626 (–C=N–). Anal. Calc. for $C_{36}H_{40}N_2$, %: C, 86.35; H, 8.05; N, 5.59. Found, %: C, 86.18; H, 7.98; N, 5.65.

Synthesis of ligand **b** as a dark yellow solid, results in the yield 92%. ^{1}H NMR ($CDCl_3$, 100 MHz), δ_H, ppm: 2.1 (6H, s), 2.35 (6H, s), 6.8–7.0 (4H, m), 7.2 (2H, d), 7.5 (2H, d), 7.85–8.00 (4H, m). MS (EI, *m/z*): 470 [M^+, 100%]. FTIR (KBr, cm^{-1}): 1277 (–C–N–), 1643 (–C=N–). Anal. Calc. for

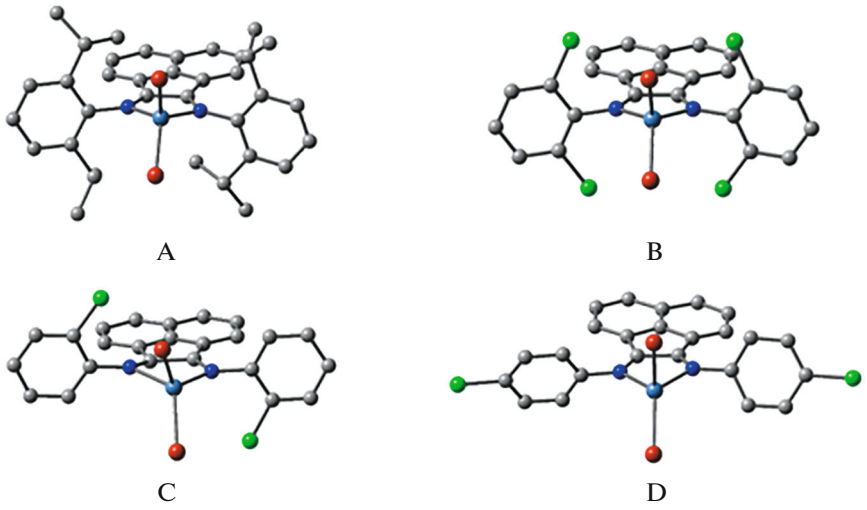

Fig. 1. Optimized structures of the precatalysts **A**–**D** (hydrogen atoms omitted for clarity).

$C_{24}H_{12}Cl_4N_2$, %: C, 61.3; H, 2.6; N, 6.0. Found, %: C, 61.2; H, 2.5; N, 6.1.

Ligand **c** as a pale green solid was obtained with the yield 91%. ^{1}H NMR ($CDCl_3$, 100 MHz), δ_H, ppm: 2.3 (6H, s), 6.8–7.1 (6H, m), 7.3–7.5 (6H, m), 8 (2H, d). MS (EI, *m/z*): 401 [M^+, 100%]. FTIR (KBr, cm^{-1}): 1278 (–C–N–), 1655 (–C=N–). Anal. Calc. for $C_{24}H_{14}Cl_2N_2$, %: C, 71.8; H, 3.5; N, 7.0. Found, %: C, 71.7; H, 3.5; N, 7.1.

Ligand **d** as a dark yellow solid was synthesized with the yield 93%. ^{1}H NMR ($CDCl_3$, 100 MHz), δ_H, ppm: 2.3 (6H, s), 6.8–7.1 (6H, m), 7.3–7.5 (6H, m), 8 (2H, d). MS (EI, *m/z*): 400 [M^+, 100%]. FTIR (KBr, cm^{-1}): 1279 (–C–N–), 1657 (–C=N–). Anal. Calc. for $C_{24}H_{14}Cl_2N_2$, %: C, 71.8; H, 3.5; N, 7.0. Found, %: C, 71.8; H, 3.4; N, 7.0.

Catalysts **A**–**D** were synthesized as brown solids. Their structures are given below:

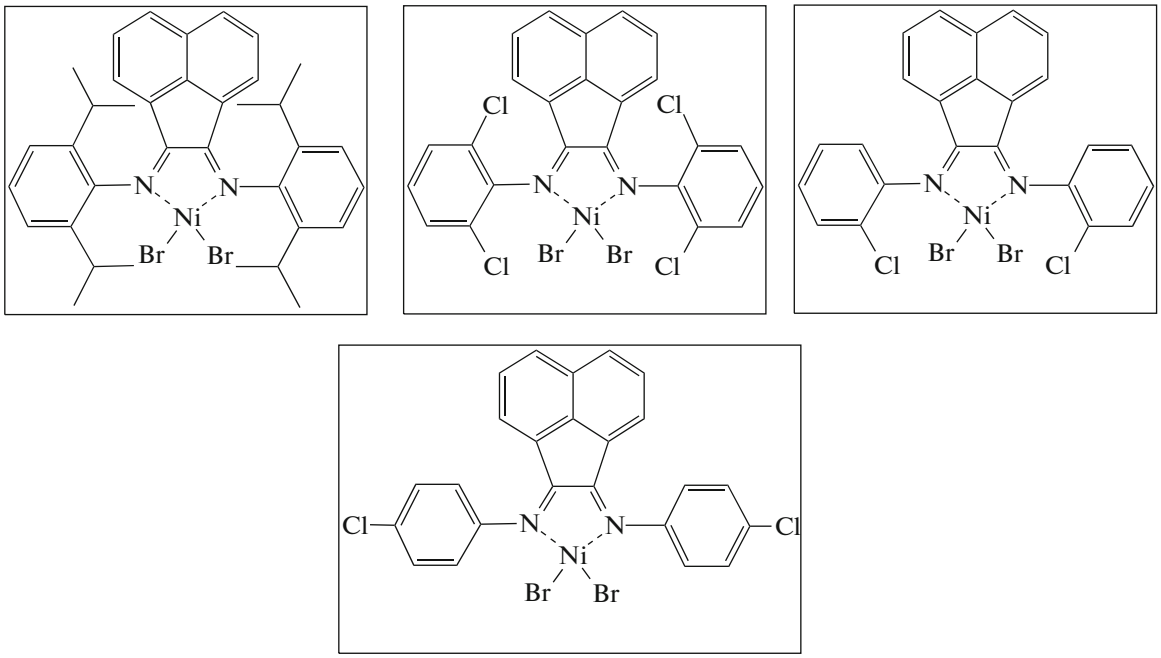

Table 1. Results of ethylene polymerization using catalyst **A** at different temperature, time and [Al]/[Ni] molar ratio[a]

Run	Catalyst	*t*, min	*T*, °C	[Al]/[Ni]	Yield, g	Activity, g PE mmol/Ni h
1	**A**	30	30	2000	3.72	2676.3
2		30	40	2000	5.65	4064.7
3		30	50	2000	7.60	5467.6
4		30	60	2000	4.50	3237.4
5		30	50	500	2.06	1482.0
6		30	50	1250	4.15	2985.6
7		30	50	3000	3.70	2661.9
8		10	50	2000	1.34	2892.1
9		20	50	2000	4.30	4640.3
10		40	50	2000	7.92	4273.4

[a] Polymerization condition: [Ni] = 2.78×10^{-3} mmol, ethylene pressure: 3.5 bar.

Table 2. Results of ethylene polymerization using catalyst **A** at different pressure

Run	*P*, bar	Yield, g	Activity, g PE mmol/Ni h	$M_v^a \times 10^5$, g/mol	ΔH^b, J/gr	$T_m{}^b$, °C	$X_c{}^b$, %
11	1	2.48	1784.2	2.8	–	–	–
3	3.5	7.60	5467.6	2.9	–	–	–
12	5	8.40	6043.2	3.2	26.8	98.2	9.1
13	6	9.07	6525.2	3.3	45.3	104.1	15.5

*Polymerization condition: [Ni] = 2.78×10^{-3} mmol. [AL]/[Ni]: 2000, time: 30 min, temperature: 50°C.
[a]Determined according to the literature [30, 31] using an Ubbelohde viscometer.
[b]Determined by DSC.

The yield of catalyst A is 95%. FTIR (KBr, cm^{-1}): the imine signal was shifted to weak field as it coordinated to the Ni; 1622 cm^{-1} (–C=N–). Anal. Calc. for $C_{36}H_{40}Br_2N_2Ni$, %: C, 60.1; H, 5.6; N, 3.9. Found, %: C, 59.6; H, 5.2; N, 3.6.

Catalyst **B** was obtained with the yield 91%. FTIR (KBr, cm^{-1}): the imine signal was shifted to weak field as it coordinated to the Ni; 1625 (–C=N–). Anal. Calc. for $C_{24}H_{12}Br_2Cl_4N_2Ni$, %: C, 55.4; H, 4.0; N, 4.6. Found, %: C, 56.5; H, 4.2; N, 4.4.

Catalyst **C** was synthesized with the yield 86%. FTIR (KBr, cm^{-1}): the imine signal was shifted to weak field as it coordinated to the Ni; 1638 (–C=N–). Anal. Calc. for $C_{24}H_{14}Br_2Cl_2N_2Ni$, %: C, 46.5; H, 2.3; N, 4.5. Found, %: C, 45.8; H, 2.1; N, 4.1.

Synthesis of catalyst **D** leads to the yield 90%. FTIR (KBr, cm^{-1}): the imine signal was shifted to weak field as it coordinated to the Co; 1628 (–C=N–). Anal. Calc. for $C_{24}H_{14}Br_2Cl_2N_2Ni$, %: C, 46.5; H, 2.3; N, 4.5. Found, %: C, 45.9; H, 2.2; N, 4.4.

RESULTS AND DISCUSSION

Ethylene Polymerization Using Catalyst A

For ethylene polymerization catalyzed by **A** (Fig. 1), the effects of reaction parameters such as cocatalyst/catalyst molar ratio, temperature, time and pressure on the catalyst performance were studied. The results are presented in Tables 1 and 2. It revealed that the catalyst activity increases as the temperature raised from 30 to 50°C. However, at higher temperature the activity decreases due to irreversible deactivation (decomposition) of the active species and decrease of ethylene solubility [8, 15, 32, 33]. The optimum value of [Al]/[Ni] molar ratio is equal to 2000. At lower catalyst concentration the excess amount of MAO can lead to formation of inactive stable catalyst···cocatalyst counter-ion and suppressing the propagation [8, 34]. The catalyst behavior in terms of polymerization time indicated that the catalyst activity increases until 30 min of polymerization which may correspond to alkylation of all active centers by co-catalyst. At later polymerization time, degradation

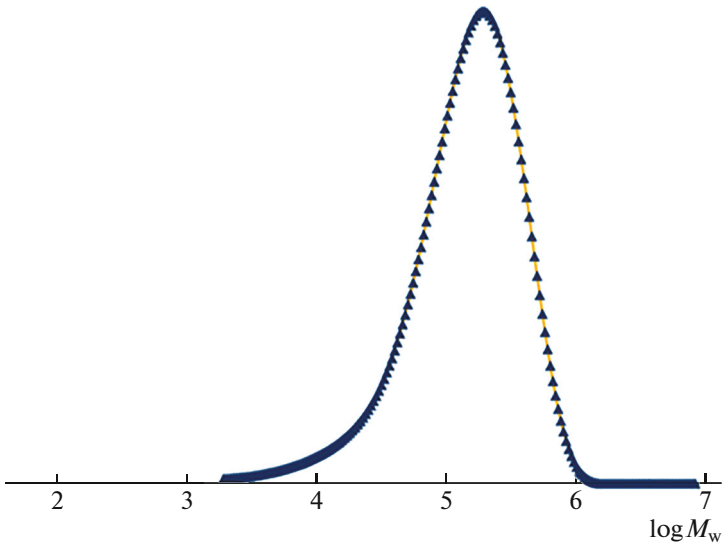

Fig. 2. GPC curve of PE sample made by catalyst **A** (Run 3).

and deactivation of active centers prevents monomer insertion and leads to decrease of catalyst activity [8, 34].

Study on the influence of monomer pressure (Table 2) showed a non-linear increasing of the catalyst productivity due to high concentration of monomer at the environment of active center accelerating the propagation/termination rate [8, 15, 32, 35]. The growth of the pressure is accompanied by the increase of melting point T_m, crystallinity X_c and molecular weight M_v. The GPC curve (Fig. 2) of sample made by catalyst **A** (run 3) shows a narrow MWD and moderate molecular weight of PE (M_w = 141 000 g/mol, $Đ$ = 2.1).

*Ethylene Polymerization Using Catalysts **B**–**D***

To study the effect of chlorine substituent number and position on the catalyst behavior, complexes **B**–**D** were used in the polymerization of ethylene at various polymerization temperatures (Table 3). The experimental results showed that catalysts **B**, **C** and **D** are almost inactive for polymerization in comparison to complex **A**. This observation is due to nature of substituents. The presence of halogens on the aryl rings deactivates the metal center in terms of electronic and steric effects [13, 31]. Moreover, position and extent of the chlorine groups revealed that the high withdrawing groups (halogens) on *ortho*-position make the centers to be inactive while the *para* position showed better impact on the catalyst activity [19, 24, 31]. However, absence of an electronic balance on the metal center is a critical point in activity of a coordination site. There are many reports on the study of ligand structure impact and catalyst behavior as mentioned before, but there is still a demand for theoretical investigation to confirm or even predict the complex behavior in the field of olefin polymerization.

Theoretical Study on the Precatalyst and Catalyst Structures

The theoretical calculations were carried out using DFT method at B3LYP level by 6-31+G basis set (by Gaussian 09W). Moreover, to compute and depict the electron densities, graphs and structures, Multi-WFN 3.1 and GaussView 5.0 programs were employed. The structures and computed results of

Table 3. Results of ethylene polymerization using catalyst **B**–**D** at different polymerization temperature[a]

Run	Catalyst	T, °C	Yield[b], g	Activity, g PE mmol/Ni h
14	**B**	10	–[c]	–[c]
15		20	–[c]	–[c]
16		30	0.02	6.5
17		40	0.03	9.0
18	**C**	10	–[c]	–[c]
19		20	0.02	5.0
20		30	0.02	7.6
21		40	0.03	9.4
22	**D**	10	0.02	7.2
23		20	0.04	14.4
24		30	0.05	18.0
25		40	0.06	21.6

[a] Polymerization conditions: [Ni]: 2.78 × 10^{-3} mmol, ethylene pressure: 1.5 bar, polymerization time: 30 min, [A]/[Ni]: 2000.
[b] The values were rounded to simplify,
[c] The values were negligible.

Table 4. Bond distances and bonding angel calculated by DFT for precatalysts and catalysts **A**–**D**

Parameters	P–A	P–B	P–C	P–D	P–E	C–A	C–B	C–C	C–D	C–E
Ni–Br	2.34	2.30	2.29	2.30	2.34	–	–	–	–	–
Ni–Me	–	–	–	–	–	1.91	1.91	1.91	1.87	1.91
Ni–N	1.90	1.94	1.94	1.94	1.90	1.96[a]	1.95[a]	1.95[a]	1.94[a]	1.96
C=N	1.30	1.31	1.31	1.31	1.31	1.30	1.31	1.31	1.30	1.30
Ni·····X[b]	3.45	4.02	4.12	–	3.45	2.50	2.39	2.35	–	2.50
Ni·····X[c]	4.18	4.03	–	–	5.45	3.86	3.94	3.96	–	3.86
Ni·····H[d]	2.50	–	3.69	3.81	2.50	1.80	–	3.79	3.12	1.79
Ni·····H[e]	3.42	–	–	3.79	6.28	3.01	–	4.70	3.69	3.01
Br–Ni–Br	94.79	92.07	91.82	91.90	94.78	–	–	–	–	–
N–Ni–N	85.20	83.59	83.70	83.84	85.14	85.43	84.78	84.77	85.74	85.37
N–N–C	127.79	126.23	126.68	127.01	126.66	126.46[a]	123.18[a]	123.42[a]	124.16[a]	126.39

P means precatalyst, C means catalyst, E means ethylene.
[a]Mean bond distance and bond angels considered.
[b]X: the nearest atoms except hydrogen (carbon or halogen) on *ortho*-position of aryl ring.
[c]X: the furthest atoms except hydrogen (carbon or halogen) on *ortho*-position of aryl ring.
[d]H: The nearest hydrogen atoms on *ortho* groups.
[e]H: The furthest hydrogen atoms on *ortho* groups.

Table 5. The parameters calculated for precatalysts and catalysts A–D

Parameters	P–A	P–B	P–C	P–D	P–E	C–A	C–B	C–C	C–D	C–E
Mulliken charge on Ni	0.430	0.271	0.432	0.613	0.425	1.099	0.650	0.735	1.072	1.04
η or band gap, eV	0.080	0.071	0.072	0.072	0.079	0.108	0.103	0.101	0.104	0.104
–μ	0.163	0.175	0.172	0.178	0.173	0.281	0.294	0.292	0.298	0.288
ω	0.166	0.216	0.206	0.219	0.189	0.366	0.420	0.421	0.430	0.398

P means precatalyst, C means catalyst, E means ethylene.

precatalysts and catalysts **A**–**D** are depicted in Fig. 1 and gathered in Table 4. Longer Ni–Br bond distance in precatalyst **A** facilitates the bond dissociation for activation and alkylation. It also can be noticed that the distances of nearest adjacent atoms (carbon and hydrogen) on the *ortho* position of aryl ring for both precatalyst and catalyst **A** are the lowest values. This issue illustrates that the electronic and steric effects of substituents are controlling the activation step. Furthermore, it also has been reported that the presence of acenaphthene group keeps bis-aryl rings away from each other and increases the N–Ni–N bond angel [36].

This effect reduces the steric effect around the active center. However, the electronic effect of acenaphthene makes the ligand to be a better π–acceptor, inducing electron deficiency on the active center and more chain transfer reactions [30, 36]. Moreover, *ortho* substituent on one position leads to producing oligomer while the presence of groups on both positions conducts polymerization [37].

It is also expressed that the ligands bearing electronegative substituents cause instability of active center reducing catalyst lifetime and through the high chain transfer reactions, it leads to production of polymer with low molecular weight [25]. The influence of *para*-position groups on bis-aryl rings implies long distance effect conducting higher catalytic activity [19, 22, 23].

Considering the experimental results, **B** and **C** are unstable due to the presence of chlorine substituents on the *ortho* position and short lifetime along with the formation of inactive form (interaction of Ni···Cl based on the theoretical data confirmed the observations), whereas **A** was active with longer lifetime. Albeit the catalyst **D** bearing *para* chlorine substituent could be effective in the polymerization but absence of the *ortho*-alkyl groups led to not showing good results. Moreover, the parameters such as charge of Mulliken on Ni revealed that high positive charge induces capturing and more diffusion of monomer toward the active site and consequently higher activity of catalyst can be obtained (Table 5). Band gaps or chemical

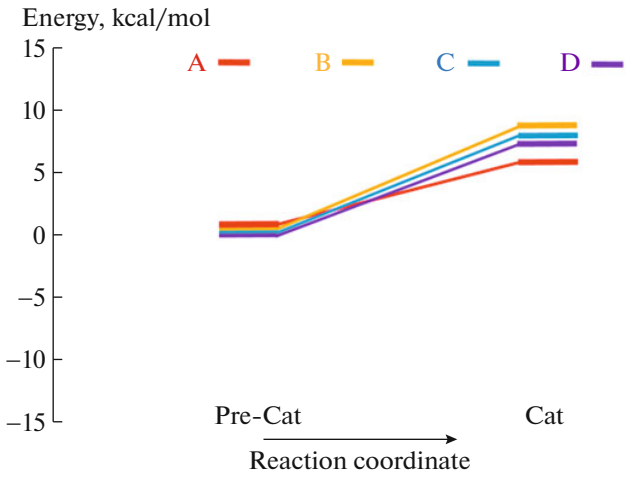

Fig. 3. Relative energy profile for precatalysts and catalysts **A**–**D**.

hardness η and electronic chemical potential μ in relation of stability and interaction energy also exhibited that higher η and -μ lead to more stability of catalyst [38, 39]. To better understanding, the precatalysts and catalysts through the alkylation reaction of complex by cocatalyst were considered in the computation. As it can be seen in Figure 3, the required energy for the activation of **A** is less than the others which is in the order of A < D < C < B.

It should be noted that in order to study on topological properties, activated form of the complexes were considered [40, 41]. The structure of each catalyst is depicted in the Cartesian coordinate system (*X*,*Y*,*Z*) containing the Ni center as the electron density and electron location function (ELF) and localized orbital locator (LOL) graphs plotted in the *XY*, *XZ*, and *YZ* planes (Figs. 4–7). These graphs clearly showed the effect of structure on the environment of active center. Regarding the *XZ* and *YZ* planes in catalyst **A** (Figs. 4b, 4c), the isopropyl groups effectively shielded the axial sites, both sides above and under the square coordination plane of Ni center [42]. This greatly retards chain transfer reactions and inhibits the latent site formation and strong $Ni^{+}\cdots$counter anion (cocatalyst) interaction [15, 43, 44]. This phenomenon also can be distinguished by the colored area around the Ni center affording higher stability and activity of the metal center. At the XY planes (Fig. 4a), the traces of electrons and orbitals of substituents can be observed which can block the equatorial sites as hindering effect. The bulky substituent on equatorial sites also suppress the chain transfer reaction and leads

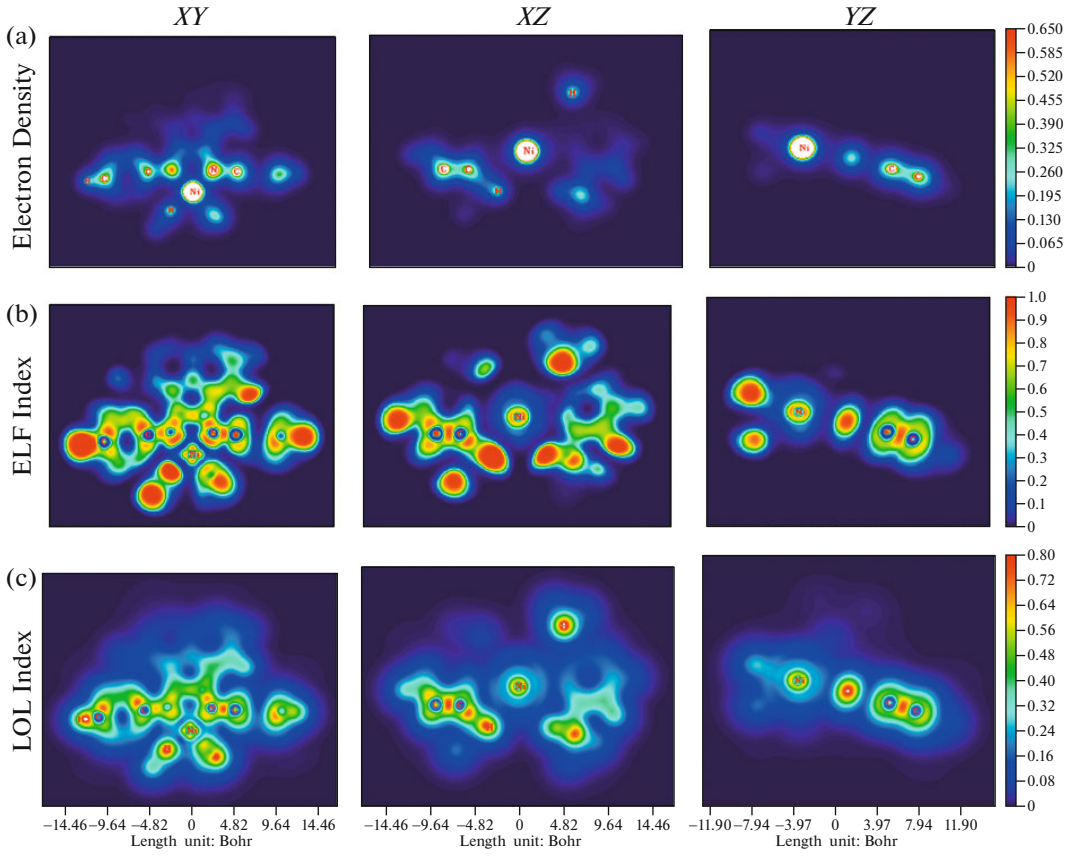

Fig. 4. Topological properties of catalyst **A**: (a) electron density, (b) ELF, and (c) LOL.

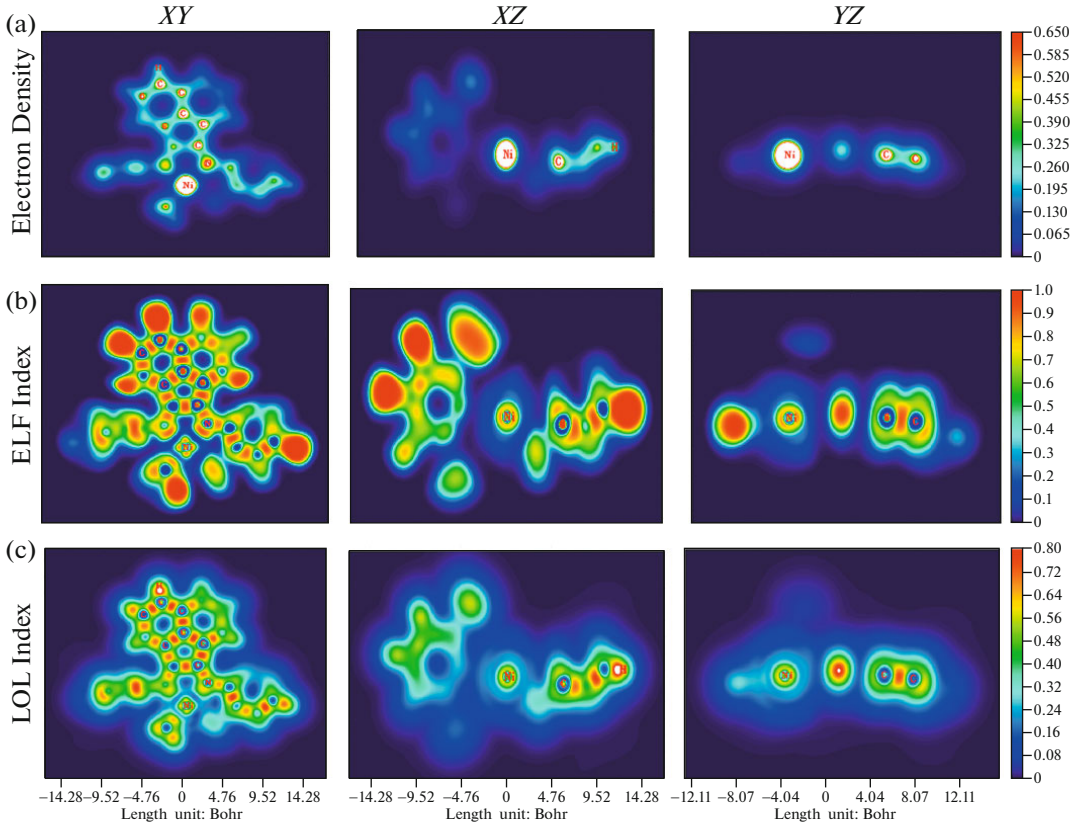

Fig. 5. Topological properties of catalyst **B**: (a) electron density, (b) ELF, and (c) LOL.

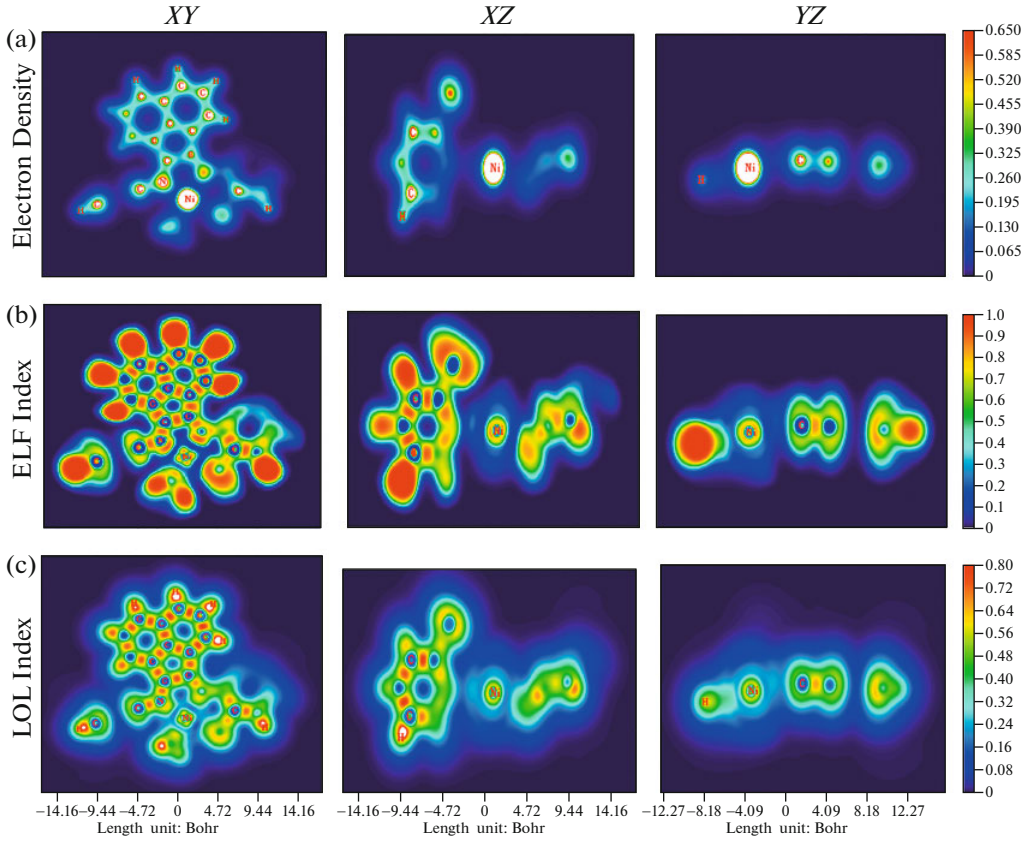

Fig. 6. Topological properties of catalyst **C**: (a) electron density, (b) ELF, and (c) LOL.

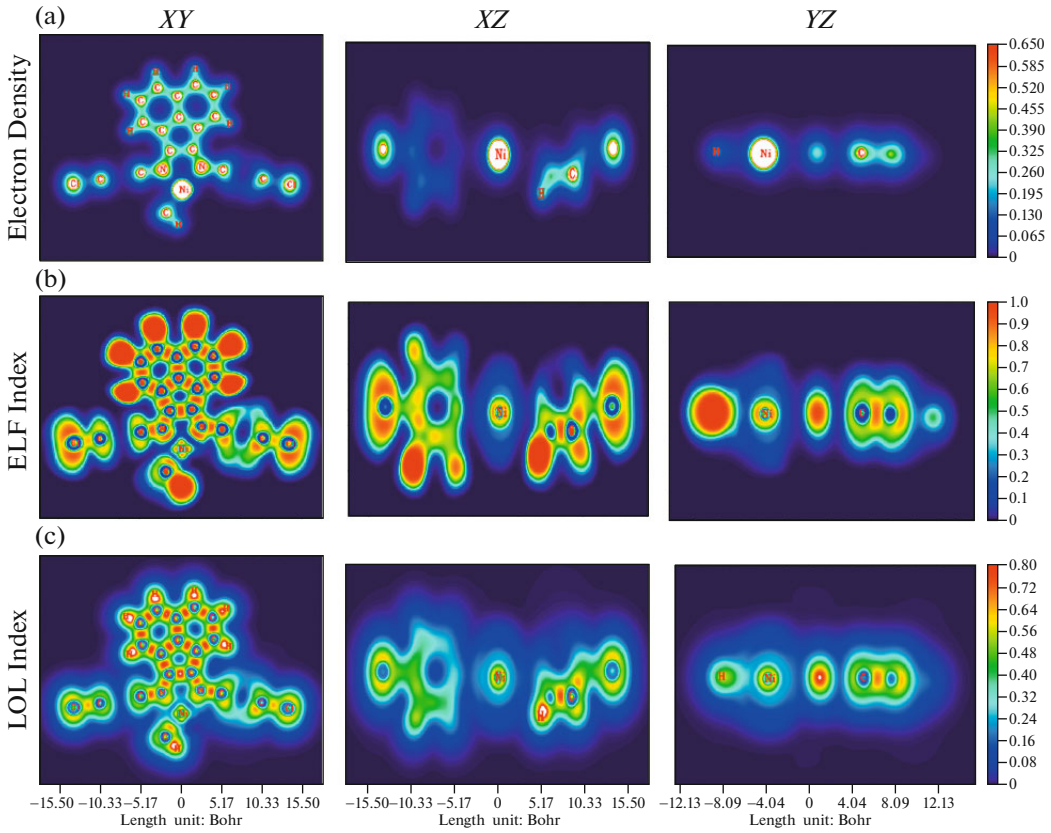

Fig. 7. Topological properties of catalyst **D**: (a) electron density, (b) ELF, and (c) LOL.

to higher molecular weight of produced polymer [45]. This point can be sterically influenced by less capability for efficient activation.

Figure 5a exhibits the structure of catalyst **B**; the *ortho*-chlorine substituent is in electrostatic interaction with the active center forming inactive site [31]. In addition to all aforementioned reasons, this interaction is suggested for almost inactivity of **B** in polymerization. This interaction is observed also for **C** (Fig. 6). As it can be observed, the electrostatic interaction of chlorine atom with cationic Ni center of catalyst **C** caused a rotation of the aryl ring and axial sites exposed to chain transfer reactions. Accordingly, the electron density and electronic effects are depleted.

The presence of withdrawing group (such as CF_3, NO_2, Cl, Br and etc.) on the *para* position has impact on the metal center even from long distance [20–25]. However, the absence of blocking groups on axial sites diminished the effect of *para*-substituent for **D**. It can be observed in the Fig. 7.

CONCLUSIONS

Four α-diimine Ni-based catalysts were synthesized and used in the polymerization of ethylene. The effect of substituent nature and position on the catalyst behavior revealed that the catalyst **A**, bearing isopropyl groups on the *ortho* position has the highest activity while for the *ortho* and *para* chlorine positioned catalysts **B–D**, insignificant activities observed. The experimental results were confirmed by the theoretical study. This part of investigation revealed that if the bond distances and bond angles be high (P–A), the complex may be alkylated by cocatalyst efficiently and feasibly. Higher charge on the metal center along with the effective shielding axial sites can cause higher monomer insertion into the growing chain. The other parameters such as η, μ and ω are in relation to the (pre)catalyst energy, that higher stable species show lower reactivity. In the other side, steric and electronic effects of substituent on the axial and equatorial sites, electronic density, ELF and LOL indicators as topological properties exhibited an impressive blocking axial sites through the orientation of aryl rings, *ortho* substituent and electronic environment for catalyst **A**, above and under the square coordination plane. The presence of chlorine atom on the *para* position could be effective if the axial site well shields by *ortho* substituents.

FUNDING

The authors are thankful of Ferdowsi University of Mashhad (FUM) and Iran Polymer and Petrochemical Institute (IPPI) for all their cooperation.

CONFLICT OF INTEREST

The authors declare that they have no conflict of interest.

REFERENCES

1. C. Bianchini, G. Giuliano, I. G. Rios, G. Mantovani, A. Meli, and A. M. Segarra, Coord. Chem. Rev. **11**, 1391 (2006).
2. M. C. Baier, M. A. Zuideveld, and S. Mecking, Angew. Chem., Int. Ed. **37**, 9722 (2014).
3. R. Gao, W. H. Sun, and C. Redshaw, Catal. Sci. Technol. **3**, 1172 (2013).
4. L. Y. Ustynyuk and B. M. Bulychev, J. Organomet. Chem. **793**, 160 (2015).
5. G. Luo, Y. Luo, Z. Hou, and J. Qu, Organometallics. **5**, 778 (2016).
6. M. Khoshsefat, N. Beheshti, G. H. Zohuri, S. Ahmadjo, and S. Soleimanzadegan, Polym. Sci, Seri. B **5**, 487 (2016).
7. C. J. Stephenson, J. P. McInnis, C. Chen, M. P. Weberski, Jr., A. Motta, M. Delferro, and T. J. Marks, ACS Catal. **3**, 999 (2014).
8. M. Khoshsefat, G. H. Zohuri, N. Ramezanian, S. Ahmadjo, and M. Haghpanah, J. Polym. Sci., Part A: Polym. Chem. **18**, 3000 (2016).
9. J. Ramos, A. Muñoz-Escalona, V. Cruz, and J. Martínez-Salazar, Polymer **7**, 2177 (2003).
10. M. Khoshsefat, A. Dechal, S. Ahmadjo, S. M. M. Mortazavi, G. H. Zohuri, and J. B. P. Soares, New J. Chem. **22**, 18288 (2018).
11. M. Khoshsefat, A. Dechal, S. Ahmadjo, S. M. M. Mortazavi, G. H. Zohuri, and J. B. P. Soares, Appl. Organomet. Chem. **6**, e4929 (2019).
12. J. Merna, Z. Hošt'álek, J. Peleška, and J. Roda, Polymer **21**, 5016 (2009).
13. M. Mogheiseh, G. H. Zohuri and M. Khoshsefat, Macromol. React. Eng. **5**, 1800006 (2018).
14. H. Terao, A. Iwashita, N. Matsukawa, S. Ishii, M. Mitani, H. Tanaka, and T. Fujita, ACS Catal. **4**, 254 (2011).
15. Z. Chen, M. Mesgar, P. S. White, O. Daugulis, and M. Brookhart, ACS Catal. **2**, 631 (2014).
16. S. Dai, S. Zhou, W. Zhang, and C. Chen, Macromolecules **23**, 8855 (2016).
17. H. Hu, H. Gao, D. Chen, G. Li, Y. Tan, G. Liang, and Q. Wu, ACS Catal. **1**, 122 (2014).
18. J. Zhang, S. Liu, A. Li, H. Ye, and Z. Li, New J. Chem. **8**, 7027 (2016).
19. J. Liu, Y. Li, Y. Li, and N. Hu, J. Appl. Polym. Sci. **2**, 700 (2008).
20. A. A. Antonov, N. V. Semikolenova, V. A. Zakharov, W. Zhang, Y. Wang, W. H. Sun, E. P. Talsi, and K. P. Bryliakov, Organometallics **3**, 1143 (2012).
21. M. Helldörfer, W. Milius, and H. G. Alt, J. Mol. Catal. A: Chem. **1**, 1 (2003).
22. J. Yuan, F. Wang, B. Yuan, Z. Jia, F. Song, and J. Li, J. Mol. Catal. A: Chem. **370**, 132 (2013).
23. F. Wang, J. Yuan, Q. Li, R. Tanaka, Y. Nakayama, and T. Shiono, Appl. Organomet. Chem. **7**, 477 (2014).
24. J. Yuan, X. Wang, T. Mei, Y. Liu, C. Miao, and X. Xie, Transition Met. Chem. **4**, 433 (2011).
25. T. K. Woo and T. Ziegler, J. Organomet. Chem. **1**, 204 (1999).
26. S. Ahmadjo, S. Damavandi, G. H. Zohuri, A. Farhadipour, and Z. Etemadinia, J. Organomet. Chem. **835**, 43 (2017).
27. C. L. Song, L. M. Tang, Y. G. Li, X. F. li, J. Chen, and Y. S. Li, J. Polym. Sci., Part A: Polym. Chem. **6**, 1964 (2006).
28. A. Dechal, M. Khoshsefat, S. Ahmadjo, S. M. M. Mortazavi, G. H. Zohuri, and H. Abedini, Appl. Organomet. Chem. **6**, e4355 (2018).
29. S. A. Sangokoya, EP Patent No. 0463555 B1 (1996).
30. M. Khoshsefat, S. Ahmadjo, S. M. M. Mortazavi, G. H. Zohuri, and J. B. P. Soares, New J. Chem. **42**, 8334 (2018).
31. S. Ahmadjo, S. Damavandi, G. H. Zohuri, A. Farhadipour, N. Samadieh, and Z. Etemadinia, Polym. Bull. **9**, 3819 (2017).
32. D. P. Gates, S. A. Svejda, E. Onate, C. M. Killian, L. K. Johnson, P. S. White, and M. Brookhart, Macromolecules **7**, 2320 (2000).
33. M. Khoshsefat, A. Dechal, S. Ahmadjo, S. M. M. Mortazavi, G. H. Zohuri, and J. B. P. Soares, Eur. Polym. J. **119**, 229 (2019).
34. E. Rahimipour, G. Zohuri, M. Kimiaghalam, and M. Khoshsefat, Inorg. Chim. Acta. **502**, 119354, (2020).
35. N. Nabizadeh, G. H. Zohuri, M. Khoshsefat, N. Ramezanian, and S. Ahmadjo, Polym. Sci., Ser. B **60**, 122 (2018).
36. D. H. Camacho and Z. Guan, Chem. Commun. **42**, 7879 (2010).
37. C. Popeney and Z. Guan, Organometallics **6**, 1145 (2005).
38. J. J. Gilman, "Chemical Hardness," in *Chemistry and Physics of Mechanical Hardness* (Wiley, New Jersey, 2009).
39. M. Izadyar and M. Khavani, Int. J. Quantum Chem. **10**, 666 (2014).
40. H. L. Schmider, A. D. Becke, H. L. Schmider, and A. D. Becke, J. Mol. Struct. Theochem. **1**, 51 (2000).
41. R. F. W. Bader, *Atoms in Molecules. A Quantum Theory* (Oxford Univ. Press, New York, 1990).
42. M. Mogheiseh, G. H. Zohuri, and M. Khoshsefat, J. Appl. Polym. Sci. **20**, 47376 (2019).
43. Y. Kissin, *Alkene Polymerization Reactions with Transition Metal Catalysts* (Elsevier, Amsterdam, 2008).
44. L. C. Simon, C. P. Williams, J. B. Soares, and R. F. de Souza, J. Mol. Catal. A: Chem. **1**, 55 (2001).
45. L. K. Johnson, S. Mecking, and M. Brookhart, J. Am. Chem. Soc. **1**, 267 (1996).